Timing of the martian dynamo: New constraints for a core field 4.5 and 3.7 Ga ago

A. Mittelholz, C. Johnson, J. Feinberg, Benoit Langlais, R. Phillips

GEOPHYSICS

Timing of the martian dynamo: New constraints for a core field 4.5 and 3.7 Ga ago

A. Mittelholz[1]*, C. L. Johnson[1,2], J. M. Feinberg[3], B. Langlais[4], R. J. Phillips[5]

The absence of crustal magnetic fields above the martian basins Hellas, Argyre, and Isidis is often interpreted as proof of an early, before 4.1 billion years (Ga) ago, or late, after 3.9 Ga ago, dynamo. We revisit these interpretations using new MAVEN magnetic field data. Weak fields are present over the 4.5-Ga old Borealis basin, with the transition to strong fields correlated with the basin edge. Magnetic fields, confined to a near-surface layer, are also detected above the 3.7-Ga old Lucus Planum. We conclude that a dynamo was present both before and after the formation of the basins Hellas, Utopia, Argyre, and Isidis. A long-lived, Earth-like dynamo is consistent with the absence of magnetization within large basins if the impacts excavated large portions of strongly magnetic crust and exposed deeper material with lower concentrations of magnetic minerals.

INTRODUCTION

Global magnetic fields are intimately tied to a planet's interior, surface, and atmospheric evolution. For terrestrial planets, magnetization acquired by rocks in an ancient field can be preserved over billions of years and thus provide a window into a planet's earliest history. Mars has no current global magnetic field; however, magnetic field measurements made by the Mars Global Surveyor (MGS) spacecraft (*1*) in orbit around the planet unequivocally demonstrated the presence of rocks magnetized in a past dynamo field. The first billion years of Mars' history [from ~4.5 to 3.6 billion years (Ga) ago] included massive volcanism forming most of the volume of the Tharsis province by ~3.9 Ga ago (*2*), the formation of major impact basins such as Hellas, Argyre, Isidis, and Utopia, and atmospheric and climatic conditions very different from those today as evidenced via surface morphological signatures such as valley networks (*3*) and erosional features (*4*).

Establishing the timing and duration of the martian magnetic field, relative to these major events in martian history, is critical to, e.g., understanding whether large impacts played a role in initiating (*5*) or inhibiting (*6*) a dynamo, or whether the change in surface climatic conditions after ~3.7 Ga ago (*3*) was linked to the cessation of a core dynamo. Most hypotheses regarding timing of the martian dynamo are based on the presence of magnetic fields over the heavily cratered southern hemisphere and their absence over the interiors of the large basins: Hellas, Argyre, and Isidis (*1*, *7*–*9*). An "early" dynamo [e.g., (*1*, *7*, *8*)] that had ceased by the time of basin excavation around 3.9 Ga ago (Fig. 1) remains the most accepted scenario. In this interpretation, the unmagnetized basin interiors and magnetized exteriors result from demagnetization within the basin during its formation in the absence of a global field. Furthermore, in this scenario, although a dynamo is inferred to have been present at the timing of formation of ~4.2- to 4.3-Ga old basins (*7*), the earliest history of the dynamo field was unknown. A "late" dynamo that started (*9*) after basin formation has also been proposed (Fig. 1) based on magnetic signals observed over younger volcanoes and lava flows (*10*–*13*), active or emplaced after 3.9 Ga ago. Although such spatial correlations are suggestive, a critical limitation is that it has not been possible to identify whether buried units of unknown age (likely predating 3.9 Ga ago) or datable surficial units give rise to the magnetic field signatures (*10*).

Here, we present new constraints on the timing and strength of the martian dynamo from Mars Atmosphere and Volatile EvolutioN (MAVEN) magnetic field data (*14*) acquired globally at altitudes as low as ~130 km at night [(*15*); table S1]. These data reveal a high-fidelity, high–spatial resolution (*15*, *16*) picture of the martian crustal magnetic field (table S1 caption and fig. S1) that allows detection of signals too weak or wavelengths too short to have been observed by MGS. We use nighttime MAVEN data collected below 200 km altitude to demonstrate that a dynamo likely operated at the time of formation of the northern hemisphere lowlands and the dichotomy boundary, providing new information on the earliest existence of a global magnetic field. Furthermore, we provide the first identification of a datable surface unit as the source of martian magnetization that postdated major basin formation. We suggest scenarios for the martian dynamo that can reconcile these observations with the strong magnetizations in the southern hemisphere and the absence of magnetic fields over the major basins.

RESULTS

Northern hemisphere, an early dynamo

The earliest known feature on Mars is the dichotomy boundary, at which strong magnetic signatures present in the southern hemisphere end abruptly (Fig. 2) (*1*). MGS results showed hints of weak signals over the northern hemisphere, but these were near the noise level of MGS-based models (*17*, *18*). MAVEN data clearly reveal short-wavelength, low-intensity magnetic fields over the northern hemisphere (Fig. 2 and fig. S1). These can also be seen in a new MAVEN-based model (*16*) but have not been previously discussed. Some, located around longitudes 180° to 200°, have no correlation with surface geological features and do not have a distinct gravity signal (fig. S2). Others are concentrated around the rim of the Utopia basin but are absent within the basin interior.

The spatial distribution and the strength of the magnetic fields over the northern hemisphere, as well as the transition in field strength across the dichotomy boundary, support the interpretation

[1]Department of Earth, Ocean and Atmospheric Sciences, The University of British Columbia, Vancouver, Canada. [2]Planetary Science Institute, Tucson, AZ 85719, USA. [3]Institute for Rock Magnetism, Department of Earth and Environmental Sciences, University of Minnesota, Minneapolis, MN 55455, USA. [4]Laboratoire de Planétologie et Géodynamique, UMR 6112, Université de Nantes, Université d'Angers, CNRS, 44000 Nantes, France. [5]Department of Earth and Planetary Sciences, and McDonnell Center for the Space Sciences, Washington University in St. Louis, St. Louis, MO 63130, USA. *Corresponding author. Email: amittelh@eoas.ubc.ca

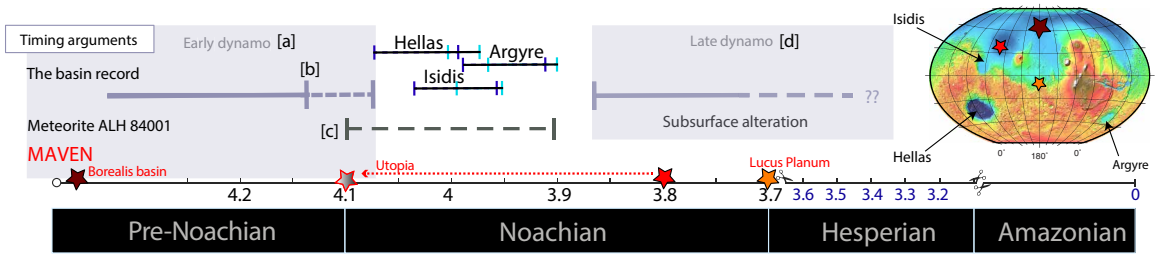

Fig. 1. Dynamo timing scenarios. An early dynamo "[a]" predating Hellas, Isidis, and Argyre (*1*). The basin age range is shown according to the isochron (cyan) and N(50) (blue) age (*47*). Early dynamo termination by 4.13 Ga "[b]" is based on magnetic field signatures of a larger basin population (*7*, *8*). The age of magnetization of meteorite ALH84001 [3.9 to 4.1 Ga; (*48*)] overlaps the early dynamo time frame "[c]." A late dynamo "[d]" postdating the major basins (*9*–*13*). New constraints from MAVEN data (stars) over the BB, around the Utopia basin, and LP that indicate a dynamo at ~4.5 and ~3.7 Ga. The timing of Utopia is uncertain (dotted line). The map displays Mars Observer Laser Altimeter topography (*49*) with BB, Utopia, and LP marked (stars).

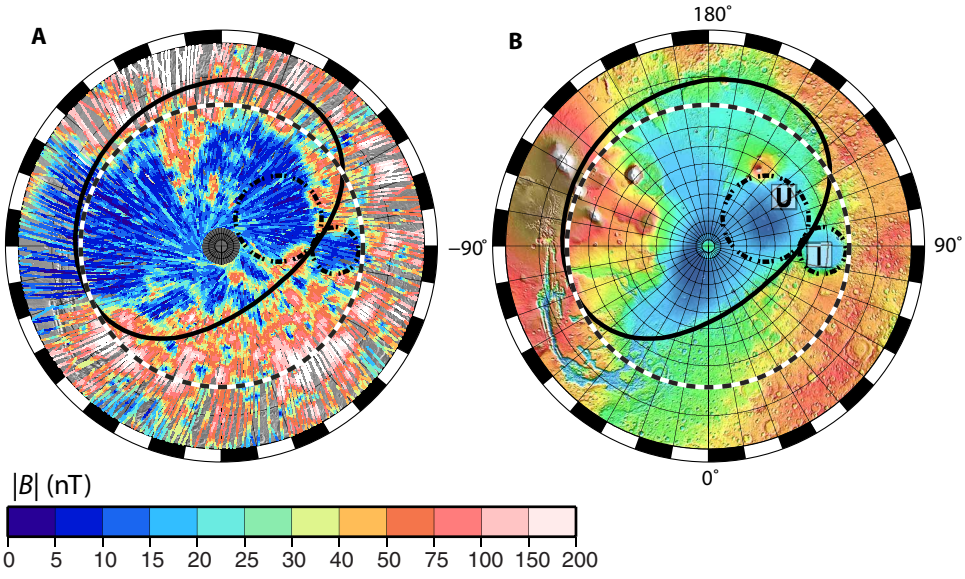

Fig. 2. Northern hemisphere observations. (**A**) Magnetic field strength, |*B*|, from all nighttime MAVEN tracks at altitudes less than 200 km. (**B**) MOLA topography (*49*). Polar stereographic projection from 20°S to the North pole, showing the basins Borealis (solid black ellipse), Utopia (U), and Isidis (I) (dashed-dotted circles), and the equator (white-black dashed line). Uncertainties in the magnetic field from measurement error are less than 1 nT (*14*).

that a large impact (*19*, *20*) formed the Borealis basin (BB) and the dichotomy boundary 4.5 Ga ago (Fig. 2) (*21*). We propose that magnetization in the BB was acquired at the time of basin formation in the presence of a global dynamo field. The localized nature of the magnetic fields within the BB can be explained as follows. Volcanic activity at Tharsis and Elysium continued into the Amazonian (*22*), and intrusion-related reheating above the Curie temperature in the absence of a global magnetic field can explain the absence of magnetic signals over most of northern Tharsis (*23*, *24*) and around Elysium. The lack of a gravity signature associated with the magnetic signals in the BB (fig. S2) further supports the idea that the magnetization therein is not the result of extensive later intrusions or a buried basin, but that it was acquired while the BB was cooling. The presence of magnetic fields around the rim of the ~3.8-Ga old (*25*) to ~4.1-Ga old (*26*) Utopia basin and their absence within its interior are consistent with, but do not require, formation of Utopia in the absence of a global field, i.e., the early dynamo scenario (*27*). We return to this later in the context of the absence of magnetic field signals over the major basins Hellas, Utopia, Isidis, and Argyre.

A second key observation is that the northern hemisphere signals are mostly weak and only robustly detected below 200 km altitude, in contrast to the strong fields over the southern highlands. The excavation of most of the crust during the BB impact could have removed magnetic minerals capable of carrying a strong magnetization, revealing lower concentrations of less strongly magnetic lithologies (*19*). Earth's mantle has a much lower concentration of magnetic minerals than the crust (*28*, *29*) and comprises more ultramafic mineralogies. The magnetic properties of martian meteorites with ultramafic cumulate mineralogies, whose compositions are consistent with martian mantle models, have been shown to be one to two orders of magnitude weaker than those of nakhlites or basaltic shergottites (*30*). The increase in field strength across the dichotomy boundary then reflects the transition in crustal and magnetic properties associated with the edge of the BB. If the martian dynamo were active at the time of the impact, then impact- and decompression-generated melts would nucleate and grow some magnetic minerals capable of recording this field as the magma differentiated, cooled, and solidified. The thermoremanent magnetization (TRM) susceptibility of these cooled melts would likely be different from the magnetic

properties of the crustal ejecta carried southward. The final magnetization would depend strongly on both the bulk chemistry of the melt (likely different from and depleted in volatiles, relative to the pre-BB martian crust) and the intensity and stability of the martian dynamo. For example, the existence of a single hemisphere dynamo that would only produce strong magnetic fields in the south as suggested in (*31*) would also allow weak and patchy magnetizations to form in the northern hemisphere. Furthermore, as proposed in (*31*), a hemispheric field could actually result from the thermal conditions in the mantle produced during the formation of the dichotomy; i.e., the BB could give rise to both hemispheric heterogeneities in the magnetic structure of the crust and hemispheric structure in the ambient field. The extent to which the strong magnetization of the southern hemisphere crust reflects magnetization that predated, but was unaffected by, the BB formation or magnetization acquired or modified during/after the BB-forming impact by the ejecta and deposition of material is unknown. In summary, the sharp spatial correlation of the transition from weaker to stronger anomalies associated with the dichotomy boundary suggests that either a thinner magnetic source layer or a different magnetic mineralogy plays a role in explaining the northern hemisphere observations, possibly aided by a weak ambient field, at least in the northern hemisphere, at the time of the BB formation (*31*).

Lucus Planum, a late dynamo

We focus next on magnetic field observations at Lucus Planum (LP), interpreted as pyroclastic flows in the Medusa Fossae Formation sourced by Apollinaris Patera (AP) (*32*). Stratigraphically, LP is divided into an upper unit, the Amazonian and Hesperian transition unit, (AHtu), and a lower unit, the Hesperian transition unit (Htu) (*22*). The Htu unit globally has a ±1-σ model age range of 3.71 to 3.96 Ga old (*22*) and, in the LP region, a model age of $3.69^{+0.05}_{-0.07}$ Ga old (hereafter 3.7 Ga old), obtained from crater counts on Htu exposures in nearby occurrences of the Medusae Fossae Formation (*33*). Htu is up to ~1.5 km thick (Fig. 3E) and is overlain in places by a thin (less than 200 m thick) younger unit AHtu (Fig. 3; see the Supplementary Materials), which is 3.49 Ga old with a ±1-σ range of 1.39 to 3.64 Ga old (*22*). In what follows, "LP" refers to just the lower Htu unit.

MGS data above AP (fig. S3) have been interpreted as evidence for a late dynamo (*11*, *12*), although the low-altitude data were argued to be contaminated by external fields (*34*). Critically, it was not possible to identify whether the datable, young surface unit or an underlying unit of different age carries the magnetization (*7*, *34*).

Long-wavelength MAVEN data also show signals spatially associated with LP and AP (Fig. 3A); nevertheless, the same source depth problem persists. However, several low-altitude MAVEN tracks lie close to a fresh-looking, ~35-km-diameter crater that penetrates the Htu flows. The AHtu unit is not present in the vicinity of the fresh crater. A 75% decrease in $|B|$ (Fig. 3B) and a change in sign of the radial field component, B_r (Fig. 3C), are observed, suggesting a change in magnetization across the crater. This is supported by a recent global model that shows a local minimum in the surface field spatially associated with the crater (fig. S4) (*16*). The elevation of the crater floor is approximately coincident with the base of the Htu unit (Fig. 3, D and E), indicating that the 1- to 1.5-km-deep crater locally penetrates most or all of this unit. The inferred crater depth is also consistent with depth-diameter, *d*/*D*, predictions (*35*). For the "deepest" complex craters in volcanic terrain, d = 1.89 km for D = 35 km, and for "all" craters, d = 1.04 km (*35*).

We tested whether the observed reduced field amplitudes over the crater could reflect demagnetization associated with the crater and its immediate surroundings. We set up a forward model in which a cylindrical hole (representing the crater and disrupted material in the surroundings) was placed in a homogeneously magnetized layer estimated from a local inversion (see Materials and Methods; fig. S5), representing the Htu unit (see Materials and Methods). The model predicts up to a 60% decrease in field strength, explaining most of the observed signal (fig. S6). This test, combined with the spatial association of magnetic field signal with the LP flow (fig. S3), indicates that a substantial fraction of the magnetization is carried within the LP unit and can be associated with a datable unit for the first time. If the pyroclastic flow acquired a thermal remanence during its emplacement, these results suggest that a martian dynamo was operating 3.7 Ga ago, after formation of the large basins.

The terrains surrounding LP show non-zero magnetization, suggesting that some magnetization may be carried by units below the surficial LP pyroclastic flow. We estimated this for the Late Amazonian volcanic (lAv) unit to the northwest and the HNt unit to the northeast of LP (Fig. 4A) to isolate the magnetization associated with LP (Fig. 4 caption). For a 1- to 2-km-thick LP layer, the magnetization bounds are 8 to 32 A/m. Natural remanent magnetization (NRM) intensities of terrestrial pyroclastic flows and martian synthetic basalts (*36*) as well as estimated NRMs of martian meteorites (*30*) are all comparable to magnetizations inferred for LP (Fig. 4C). The magnetization, M, is related to the field strength in which the flow cooled ($B_{ancient}$) and the thermoremanent magnetic susceptibility, χ_{TRM}, by $B_{ancient} = M\mu_0/\chi_{TRM}$, where μ_0 is the magnetic permeability of free space. For TRM susceptibilities of 0.1 to 1, compatible with the higher NRMs in terrestrial pyroclastic flows, an Earth-like ancient field strength is plausible (Fig. 4B).

DISCUSSION

Reinterpretation of weak basin magnetizations on Mars

Our results demonstrate that the martian dynamo was active 4.5 and 3.7 Ga ago. The existence of a dynamo field before and after the large basins Hellas, Utopia, Isidis, and Argyre requires an explanation for the general absence of magnetic fields over those basins. The impact demagnetization hypothesis is based on the argument that magnetization is absent within, but present around, the basin. Although this is true, unexplained observations worth noting are as follows: (i) Large tracts of Noachian crust surrounding the basins Hellas and Argyre are also unmagnetized or very weakly magnetized (fig. S7). Shock demagnetization can affect the basin exterior (*27*) but fails to explain the heterogeneity of magnetization around the basin or the extensive Noachian aged areas in the southern hemisphere with similarly weak or no magnetization. (ii) Short-wavelength signatures may be present in the interior of the basins (fig. S7) (*16*, *17*), although lower-altitude tracks or surface measurements are necessary to confirm this.

Can the absence of magnetic field signatures over the basins be explained if a dynamo was operating during basin formation? At least two possibilities exist: (i) The giant impacts excavated large fractions of the crust, possibly removing material capable of carrying strong magnetizations. For crater diameters, D, up to ~500 km, the excavation depth, d, is ~0.1D, i.e., up to 50 km (*37*). Transient crater diameter estimates for Argyre, Isidis, and Hellas range from 750 to 1400 km (*38*). Although the *d*/*D* ratio for such large basins is

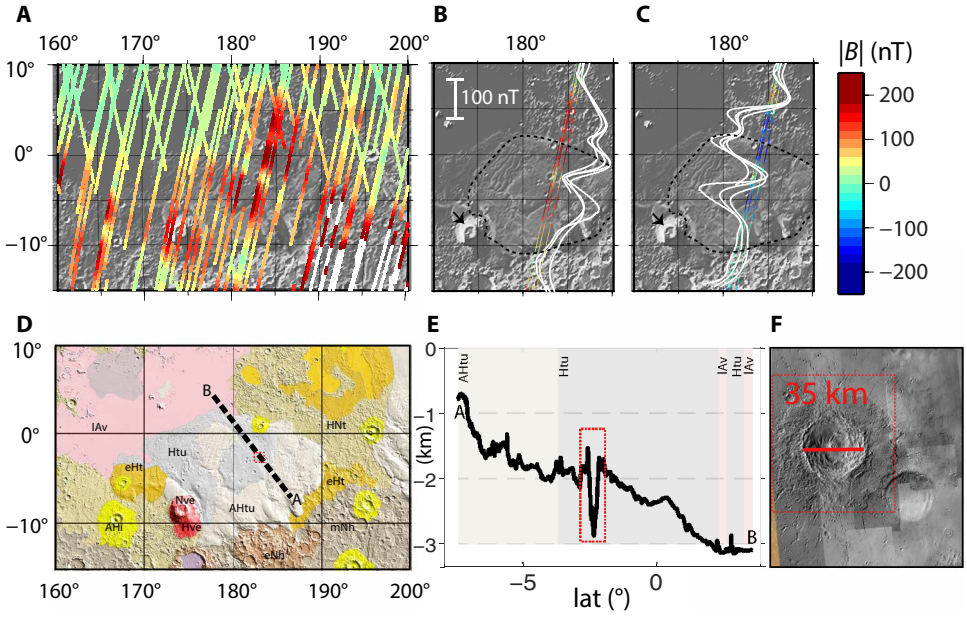

Fig. 3. LP observations. (**A** to **C**) Magnetic field over AP and LP below 200 km altitude. (A) $|B|$ from MAVEN nighttime tracks. (B) $|B|$ and (C) B_r along four tracks close to the fresh LP crater. AP and LP are indicated by arrows and dashed black lines, respectively. The magnetic field is shown by the colors along the tracks. The white wiggles show $|B|$ and B_r as a function of distance along the track, and the scale bar in (B) denotes the amplitude. (**D**) Geological map (*22*) with track for topographic profile shown in (**E**). (**F**) A Mars Reconnaissance Orbiter Context Camera (CTX, 6 m/pixel resolution) image of the fresh crater highlighted by the red box in (D) and (E). Unit abbreviations are as follows: eNh, Early Noachian highland; HNt, Hesperian and Noachian transition; eHt, Early Hesperian transition; mNh, Middle Noachian highland; Nve, Noachian volcanic effusive; Hve, Hesperian volcanic effusive.

uncertain, the depths would exceed 50 km, effectively penetrating and removing magnetized crust. The observations of very weak fields over the BB, cf. the surrounding southern highlands, suggest that this is plausible. Weak, small-scale signals may exist within the Argyre, Isidis, Hellas, and Utopia basins but require more lower-altitude observations for definitive identification. Material excavation, with only weak or small-scale subsequent magnetization, would produce a magnetic field signature at MGS and MAVEN altitudes barely distinguishable from basin-localized demagnetization. (ii) We also cannot exclude a fortuitous scenario in which a dynamo field at the time of basin formation was substantially weakened or intermittent, as a result of a reversing dynamo field (*39*). (iii) Alternatively, the dynamo was inactive during the time of basin formation, for example, because of inherently changing dynamo processes (i.e., from a thermally to a compositionally driven dynamo).

Implications of a dynamo 4.5 and 3.7 Ga ago

Evidence for a dynamo both ~4.5 and ~3.7 Ga ago has major implications for Mars' evolution. Assuming a thermo-chemically driven magnetic dynamo, Mars must have sustained sufficiently vigorous core convection at its very earliest times and at the time of LP flow emplacement. Furthermore, the observations at LP suggest that a substantial fraction of the magnetization is carried in a thin, shallow magnetized unit. The resulting magnetizations are consistent with magnetization of pyroclastic flows in a 3.7-Ga old surface field with a strength similar to that of Earth's present field. Excavation during large impacts may have played a key role in establishing a heterogeneous distribution of magnetic carriers in the martian crust, particularly removing magnetic minerals from the interior of major basins. This scenario allows a dynamo to plausibly persist from 4.5 to 3.7 Ga ago, thereby opening the possibility for a range of new magnetization processes to affect the martian surface, including depositional and crystallization remanence. For example, morphological evidence for water in the form of valley networks at the surface of Mars is dated between the Noachian and the Early Hesperian (*3*), before and overlapping with the timing of formation of LP and hence the dynamo. Water circulating in the martian crust in the presence of a field could have resulted in hydrothermal alteration facilitating magnetization or remagnetization of magnetic minerals (*40*).

Furthermore, the results link to current and planned missions' e.g., the interior structure is a primary goal of the InSight mission currently operating on the martian surface (*41*). The dynamo timing results presented here provide a major step forward in understanding Mars' thermal evolution, especially when combined with existing constraints on heat flow, mantle temperature, interior composition, and physical models of structure of the martian core. Also, if a global magnetic field protects the atmosphere from solar wind energetic particles, a prolonged dynamo would delay the effects of some of the atmospheric removal processes and hence have implications for martian atmospheric loss rates (*42*). This is important for addressing one of the main MAVEN goals of atmospheric escape rates through time (*42*). The collection of martian samples and their return to the Earth will finally be underway with sample collection by the Mars 2020 rover to be launched next year. An extended dynamo, consistent with the new results here, is of key importance for the Jezero landing site selected for Mars 2020, because units that could be sampled might have formed at a time of an active dynamo field (*43*). Future laboratory investigation of return samples will be the next major step in Mars exploration and, if magnetized, for planetary paleomagnetism.

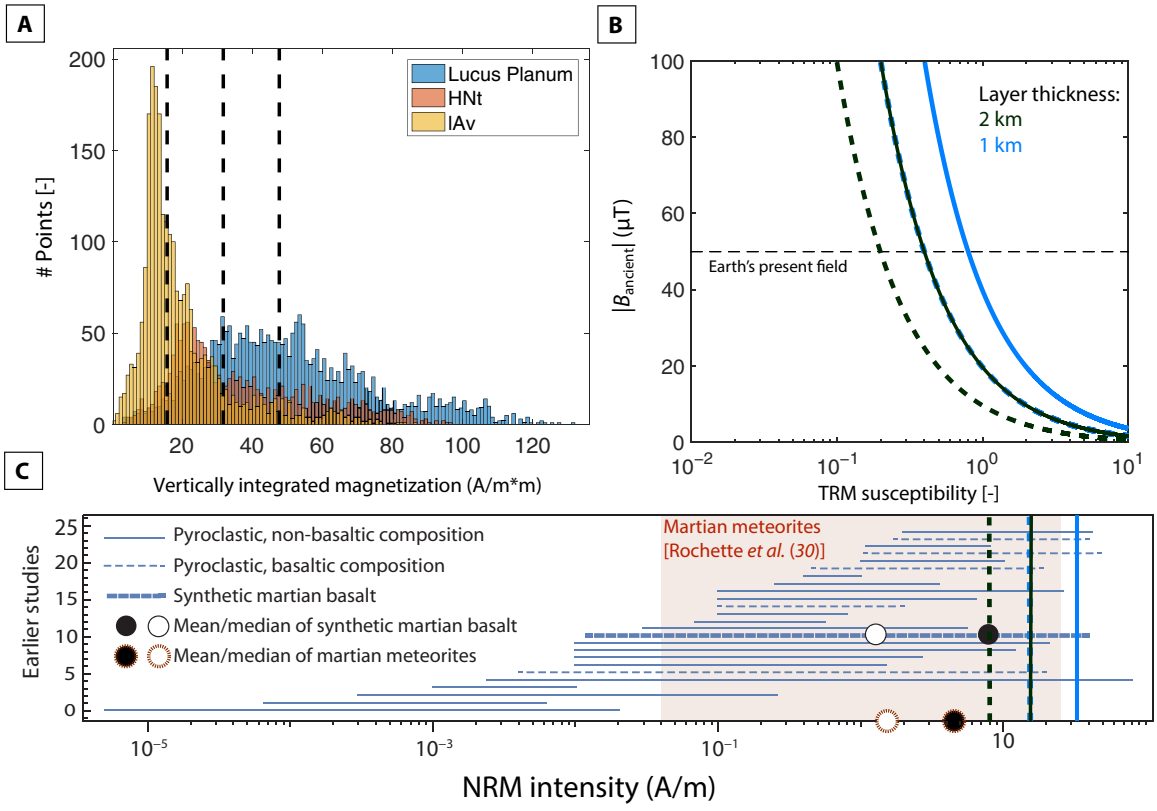

Fig. 4. Magnetization of LP. (**A** and **B**) The distributions of vertically integrated magnetization spatially associated with the Htu and AHtu units of LP (blue) as well as the HNt (brown) and lAv (yellow) units. The dashed lines represent the median for each distribution (15.7, 31.7, and 47.7 A for lAV, HNt, and LP, respectively). (B) Resulting estimations of the ancient field strength for LP layer thicknesses of 1 and 2 km versus thermoremanent susceptibility, χ_{TRM}, after subtraction of the median values of the vertically integrated magnetizations underlying the lAv and HNt from that for LP (dashed and solid lines, respectively). In SI units, χ_{TRM} is dimensionless. (**C**) Compilation of NRM intensity ranges (bottom axis) of terrestrial pyroclastic deposits (see the Supplementary Materials), martian synthetic basalts with mean and median of 1.3 and 7.7 A/m (*36*), and estimated NRMs derived from 27 martian meteorites (range in red) with a mean and median of 1.7 and 4.4 A/m [table 2 from (*30*)]. The vertical lines correspond to the lines in (B).

MATERIALS AND METHODS

Crustal field modeling

Local crustal field modeling is based on the equivalent source dipole method (*44*). The magnetized layer is represented by evenly distributed (every 90 km) dipoles placed at mid-depth of a 40-km-thick layer. Dipoles within 75° of the observation point contribute to every orbital measurement (*45*), and the inversion optimizes the misfit between satellite data and the model prediction, by solving for the direction and strength of each dipole, without overfitting noise. Our solution method is conjugate gradient least squares that minimizes the root mean square difference between the data and an iteratively fitted model. The preferred solution is picked using the corner of the L-curve (*46*). We perform the inversion 100 times with randomly selected 50% subsets of the full dataset above the model area and 10% of the data in the buffer region and present the mean of all inversions (fig. S5A) and corresponding standard deviation (fig. S5B).

We use all nighttime MAVEN data down-sampled to 1 Hz (available on the Planetary Data System) below 400 km altitude, as well as nighttime (~2 a.m.) MGS Mapping Orbit data (~400 km altitude) binned in 10-km altitude and 0.1° longitude and latitude bins. Binning of the MGS data is necessary because of the large dataset collected throughout the mapping phase of the mission (1999 to 2006). Nighttime low-altitude (<350 km) data for MGS data are not available for the modeled area.

Foward modeling

We set up a forward model in which a cylindrical hole (the crater) is placed in a homogeneously magnetized layer representing the Htu unit. Thus, we isolate the signal that is caused by the crater cavity itself while ignoring any additional signal due to heterogeneities of magnetization that we would expect in a pyroclastic flow. We use the estimated dipole moments from our inversion (fig. S6A) in the vicinity of the crater to estimate the magnetization of the Htu unit, assuming a 1.5-km-thick layer [M_r, M_θ, $M\varphi$] = [−24, 36, 7.8] A/m. This represents the near-surface layer, mapped as Htu (Fig. 3D), which is ~3.7 Ga and ~1.5 km thick. We considered a dense and broad mesh, with dipoles placed every 4 km laterally to 700 km outside our modeled region as a buffer. We allowed the crater to penetrate part of or the entire magnetized unit (i.e., we allowed a thinner magnetized layer below the crater interior) and find that the observed drop can best be modeled if the full unit is penetrated. We note that the magnitude of the LP magnetization is not critical to our calculations because we examine the percentage change in the magnetic field associated with the unmagnetized crater (the hole). The observed magnetic field east of the fresh-looking crater (fig. S5) is best explained if an adjacent crater is also demagnetized. This second crater is more degraded and is ~35 km in diameter, suggesting that it penetrates a depth similar to that of the fresh crater. The crater age is unknown; superposition relationships indicate that it is older

than the fresh crater but postdates the emplacement of the LP flow. The forward model predicts up to a 60% decrease in field strength, assuming that the demagnetization is associated with a hole 1.5 times the diameter of each crater, i.e., the width of the craters and ejecta blankets (fig. S5B), explaining most of the observed 75% decrease in the data.

SUPPLEMENTARY MATERIALS

Supplementary material for this article is available at http://advances.sciencemag.org/cgi/content/full/6/18/eaba0513/DC1

REFERENCES AND NOTES

1. M. H. Acuña, J. E. P. Connerney, N. F. Ness, R. P. Lin, D. Mitchell, C. W. Carlson, J. McFadden, K. A. Anderson, H. Rème, C. Mazelle, D. Vignes, P. Wasilewski, P. Cloutier, Global distribution of crustal magnetization discovered by the mars global surveyor MAG/ER experiment. *Science* **284**, 790–793 (1999).
2. R. J. Phillips, M. T. Zuber, S. C. Solomon, M. P. Golombek, B. M. Jakosky, W. B. Banerdt, D. E. Smith, R. M. Williams, B. M. Hynek, O. Aharonson, S. A. Hauck II, Ancient geodynamics and global-scale hydrology on Mars. *Science* **291**, 2587–2591 (2001).
3. C. I. Fassett, J. W. Head III, The timing of martian valley network activity: Constraints from buffered crater counting. *Icarus* **195**, 61–89 (2008).
4. B. M. Hynek, R. J. Phillips, Evidence for extensive denudation of the Martian highlands. *Geology* **29**, 407–410 (2001).
5. C. C. Reese, V. S. Solomatov, Early martian dynamo generation due to giant impacts. *Icarus* **207**, 82–97 (2010).
6. J. H. Roberts, R. J. Lillis, M. Manga, Giant impacts on early mars and the cessation of the martian dynamo. *J. Geophys. Res. E Planets.* **114**, E4 (2009).
7. R. J. Lillis, S. Robbins, M. Manga, J. S. Halekas, H. V. Frey, Time history of the Martian dynamo from crater magnetic field analysis. *J. Geophys. Res. E Planets* **118**, 1488–1511 (2013).
8. F. Vervelidou, V. Lesur, M. Grott, A. Morschhauser, R. J. Lillis, Constraining the date of the martian dynamo shutdown by means of crater magnetization signatures. *J. Geophys. Res. Planets* **122**, 2294–2311 (2017).
9. G. Schubert, C. T. Russell, W. B. Moore, Timing of the Martian dynamo. *Nature* **408**, 666–667 (2000).
10. R. J. Lillis, M. Manga, D. L. Mitchell, R. P. Lin, M. H. Acuna, Unusual magnetic signature of the Hadriaca Patera Volcano: Implications for early Mars. *Geophys. Res. Lett.* **33**, 3–6 (2006).
11. B. Langlais, M. Purucker, A polar magnetic paleopole associated with Apollinaris Patera, Mars. *Planet. Space Sci.* **55**, 270–279 (2007).
12. L. L. Hood, K. P. Harrison, B. Langlais, R. J. Lillis, F. Poulet, D. A. Williams, Magnetic anomalies near Apollinaris Patera and the Medusae Fossae Formation in Lucus Planum, Mars. *Icarus* **208**, 118–131 (2010).
13. C. Milbury, G. Schubert, C. A. Raymond, S. E. Smrekar, B. Langlais, The history of Mars' dynamo as revealed by modeling magnetic anomalies near Tyrrhenus Mons and Syrtis Major. *J. Geophys. Res.* **117**, E10007 (2012).
14. J. E. P. Connerney, J. R. Espley, G. A. Dibraccio, J. R. Gruesbeck, R. J. Oliversen, D. L. Mitchell, J. Halekas, C. Mazelle, D. Brain, B. M. Jakosky, First results of the MAVEN magnetic field investigation. *Geophys. Res. Lett.* **42**, 8819–8827 (2015).
15. A. Mittelholz, C. L. Johnson, A. Morschhauser, A new magnetic field activity proxy for Mars from MAVEN data. *Geophys. Res. Lett.* **45**, 5899–5907 (2018).
16. B. Langlais, E. Thébault, A. Houliez, M. E. Purucker, R. J. Lillis, A new model of the crustal magnetic field of mars using MGS and MAVEN. *J. Geophys. Res. Planet.* **124**, 1542–1569 (2019).
17. R. J. Lillis, H. V. Frey, M. Manga, D. L. Mitchell, R. P. Lin, M. H. Acuña, S. W. Bougher, An improved crustal magnetic field map of Mars from electron reflectometry: Highland volcano magmatic history and the end of the martian dynamo. *Icarus* **194**, 575–596 (2008).
18. A. Morschhauser, V. Lesur, M. Grott, A spherical harmonic model of the lithospheric magnetic field of Mars. *J. Geophys. Res. Planets.* **119**, 1162–1188 (2014).
19. M. M. Marinova, O. Aharonson, E. I. Asphaug, Mega-impact formation of the Mars hemispheric dichotomy. *Nature* **453**, 1216–1219 (2008).
20. J. C. Andrews-Hanna, M. T. Zuber, W. B. Banerdt, The Borealis basin and the origin of the martian crustal dichotomy. *Nature* **453**, 1212–1215 (2008).
21. W. F. Bottke, J. C. Andrews-Hanna, A post-accretionary lull in large impacts on early Mars. *Nat. Geosci.* **10**, 344–348 (2017).
22. K. L. Tanaka, J. A. Skinner, J. M. Dohm, R. P. Irwin, E. J. Kolb, C. M. Fortezzo, T. Platz, G. G. Michael, T. M. Hare, Geologic map of Mars, U.S. Geological Survey Scientific Investigations Map 3292 (2014); https://pubs.usgs.gov/sim/3292/.
23. C. L. Johnson, R. J. Phillips, Evolution of the Tharsis region of Mars: Insights from magnetic field observations. *Earth Planet. Sci. Lett.* **230**, 241–254 (2005).
24. R. J. Lillis, J. Dufek, J. E. Bleacher, M. Manga, Demagnetization of crust by magmatic intrusion near the Arsia Mons volcano: Magnetic and thermal implications for the development of the Tharsis province, Mars. *J. Volcanol. Geotherm. Res.* **185**, 123–138 (2009).
25. S. C. Werner, The early martian evolution—Constraints from basin formation ages. *Icarus* **195**, 45–60 (2008).
26. H. V. Frey, Impact constraints on, and a chronology for, major events in early Mars history. *J. Geophys. Res. E Planets.* **111**, 1–11 (2006).
27. R. J. Lillis, H. V. Frey, M. Manga, Rapid decrease in Martian crustal magnetization in the Noachian era: Implications for the dynamo and climate of early Mars. *Geophys. Res. Lett.* **35**, L14203 (2008).
28. E. C. Ferré, S. A. Friedman, F. Martín-Hernández, J. M. Feinberg, J. A. Conder, D. A. Ionov, The magnetism of mantle xenoliths and potential implications for sub-Moho magnetic sources. *Geophys. Res. Lett.* **40**, 105–110 (2013).
29. P. J. Wasilewski, M. A. Mayhew, The moho as a magnetic boundary revisited. *Geophys. Res. Lett.* **19**, 2259–2262 (1992).
30. P. Rochette, J. Gattacceca, V. Chevrier, V. Hoffmann, J.-P. Lorand, M. Funaki, R. Hochleitner, Matching Martian crustal magnetization and magnetic properties of Martian meteorites. *Meteorit. Planet. Sci.* **40**, 529–540 (2005).
31. S. Stanley, L. Elkins-Tanton, M. T. Zuber, E. M. Parmentier, Mars' paleomagnetic field as the result of a single-hemisphere dynamo. *Science* **321**, 1822–1825 (2008).
32. L. Kerber, J. W. Head, J.-B. Madeleine, F. Forget, L. Wilson, The dispersal of pyroclasts from Apollinaris Patera, Mars: Implications for the origin of the Medusae Fossae Formation. *Icarus* **216**, 212–220 (2011).
33. J. R. Zimbelman, S. P. Scheidt, Hesperian age for western medusae fossae formation, Mars. *Science* **336**, 1683 (2012).
34. A. Morschhauser, "A model of the crustal magnetic field of Mars," thesis, Wilhelms-Universitaet Münster (2016).
35. S. J. Robbins, B. M. Hynek, A new global database of Mars impact craters ≥ 1 km: 2 Global crater properties and regional variations of the simple-to-complex transition diameter. *J. Geophys. Res. Planets.* **117**, 1–21 (2012).
36. J. A. Bowles, J. E. Hammer, S. A. Brachfeld, Magnetic and petrologic characterization of synthetic Martian basalts and implications for the surface magnetization of Mars. *J. Geophys. Res. E Planets.* **114**, 1–18 (2009).
37. B. Langlais, E. Thébault, Predicted and observed magnetic signatures of martian (de) magnetized impact craters. *Icarus* **212**, 568–578 (2011).
38. H. J. Melosh, *Impact Cratering. A Geologic Process* (Cambridge Univ. Press, 1989), vol. 126.
39. P. Rochette, Crustal magnetization of Mars controlled by lithology or cooling rate in a reversing dynamo? *Geophys. Res. Lett.* **33**, 2006–2009 (2006).
40. K. H. Harrison, R. E. Grimm, Controls on Martian hydrothermal systems: Application to valley network and magnetic anomaly formation. *J. Geophys. Res.* **107**, 1-1–1-10 (2002).
41. S. E. Smrekar, P. Lognonné, T. Spohn, W. B. Banerdt, D. Breuer, U. Christensen, V. Dehant, M. Drilleau, W. Folkner, N. Fuji, R. F. Garcia, D. Giardini, M. Golombek, M. Grott, T. Gudkova, C. Johnson, A. Khan, B. Langlais, A. Mittelholz, A. Mocquet, R. Myhill, M. Panning, C. Perrin, T. Pike, A.-C. Plesa, A. Rivoldini, H. Samuel, S. C. Stähler, M. van Driel, T. Van Hoolst, O. Verhoeven, R. Weber, M. Wieczorek, Pre-mission InSights on the interior of Mars. *Space Sci. Rev.* **215**, 3 (2018).
42. B. M. Jakosky, R. P. Lin, J. M. Grebowsky, J. G. Luhmann, D. F. Mitchell, G. Beutelschies, T. Priser, M. Acuna, L. Andersson, D. Baird, D. Baker, R. Bartlett, M. Benna, S. Bougher, D. Brain, D. Carson, S. Cauffman, P. Chamberlin, J. Y. Chaufray, O. Cheatom, J. Clarke, J. Connerney, T. Cravens, D. Curtis, G. Delory, S. Demcak, A. DeWolfe, F. Eparvier, R. Ergun, A. Eriksson, J. Espley, X. Fang, D. Folta, J. Fox, C. Gomez-Rosa, S. Habenicht, J. Halekas, G. Holsclaw, M. Houghton, R. Howard, M. Jarosz, N. Jedrich, M. Johnson, W. Kasprzak, M. Kelley, T. King, M. Lankton, D. Larson, F. Leblanc, F. Lefevre, R. Lillis, P. Mahaffy, C. Mazelle, W. McClintock, J. McFadden, D. L. Mitchell, F. Montmessin, J. Morrissey, W. Peterson, W. Possel, J. A. Sauvaud, N. Schneider, W. Sidney, S. Sparacino, A. I. F. Stewart, R. Tolson, D. Toublanc, C. Waters, T. Woods, R. Yelle, R. Zurek, The Mars Atmosphere and Volatile Evolution (MAVEN) mission. *Space Sci. Rev.* **195**, 3–48 (2015).
43. A. Mittelholz, A. Morschhauser, C. L. Johnson, B. Langlais, R. J. Lillis, F. Vervelidou, B. P. Weiss, The Mars 2020 candidate landing sites: A magnetic field perspective. *Earth Space Sci.* **5**, 410–424 (2018).
44. M. Mayhew, Inversion of satellite magnetic anomaly data. *J. Geophys. Zeitschrift Geophys.* **45**, 119–128 (1979).
45. M. E. Purucker, T. J. Sabaka, R. A. Langel, Conjugate gradient analysis: A new tool for studying satellite magnetic data sets. *Geophys. Res. Lett.* **23**, 507–510 (1996).
46. R. C. Aster, B. Borchers, C. H. Thurber, *Parameter Estimation and Inverse Problems* (Elsevier Academic Press, ed. 2, 2011).
47. S. J. Robbins, B. M. Hynek, R. J. Lillis, W. F. Bottke, Large impact crater histories of Mars: The effect of different model crater age techniques. *Icarus* **225**, 173–184 (2013).
48. B. P. Weiss, H. Vali, F. J. Baudenbacher, J. L. Kirschvink, S. T. Stewart, D. L. Shuster, Records of an ancient Martian magnetic field in ALH84001. *Earth Planet. Sci. Lett.* **201**, 449–463 (2002).

49. D. E. Smith, M. T. Zuber, V. Frey, B. Garvin, O. Muhleman, H. Pettengill, J. Phillips, H. J. Zwally, C. Duxbury, G. Lemoine, A. Neumann, D. D. Rowlands, O. Aharonson, P. G. Ford, A. B. Iranov, L. Johnson, J. Mcgovern, B. Abshire, R. S. Afzal, X. Sun, Mars Orbiter Laser Altimeter: Experiment summary after the first year of global mapping of Mars. *J. Geophys. Res. Planets.* **106**, 23689–23722 (2001).
50. M. H. Ort, S. L. de Silva, N. C. Jiménez, B. R. Jicha, B. S. Singer, Correlation of ignimbrites using characteristic remanent magnetization and anisotropy of magnetic susceptibility, Central Andes, Bolivia. *Geochem. Geophys. Geosyst.* **14**, 141–157 (2013).
51. M. Schätz, T. Reischmann, J. Tait, V. Bachtadse, H. Bahlburg, U. Martin, The Early Palaeozoic break-up of northern Gondwana, new palaeomagnetic and geochronological data from the Saxothuringian Basin, Germany. *Int. J. Earth Sci.* **91**, 838–849 (2002).
52. E. Izquierdo-Llavall, A. Casas-Sainz, B. Oliva-Urcia, R. Scholger, Palaeomagnetism and magnetic fabrics of the Late Palaeozoic volcanism in the Castejón-Laspaúles basin (Central Pyrenees). Implications for palaeoflow directions and basin configuration. *Geol. Mag.* **151**, 777–797 (2014).
53. M. Iorio, J. Liddicoat, F. Budillon, A. Incoronato, R. S. Coe, D. D. Insinga, W. S. Cassata, C. Lubritto, A. Angelino, S. Tamburrino, Combined palaeomagnetic secular variation and petrophysical records to time-constrain geological and hazardous events: An example from the eastern Tyrrhenian Sea over the last 120ka. *Glob. Planet. Change.* **113**, 91–109 (2014).
54. C. Lesti, M. Porreca, G. Giordano, M. Mattei, R. A. F. Cas, H. M. N. Wright, C. B. Folkes, J. Viramonte, High-temperature emplacement of the Cerro Galán and Toconquis Group ignimbrites (Puna plateau, NW Argentina) determined by TRM analyses. *Bull. Volcanol.* **73**, 1535–1565 (2011).
55. M. Porreca, M. Mattei, C. MacNiocaill, G. Giordano, E. McClelland, R. Funiciello, Paleomagnetic evidence for low-temperature emplacement of the phreatomagmatic Peperino Albano ignimbrite (Colli Albani volcano, Central Italy). *Bull. Volcanol.* **70**, 877–893 (2008).
56. G. Giordano, E. Zanella, M. Trolese, C. Baffioni, A. Vona, C. Caricchi, A. A. De Benedetti, S. Corrado, C. Romano, R. Sulpizio, N. Geshi, Thermal interactions of the AD79 Vesuvius pyroclastic density currents and their deposits at Villa dei Papiri (Herculaneum archaeological site, Italy). *Earth Planet. Sci. Lett.* **490**, 180–192 (2018).
57. P. P. Lebti, J.-C. Thouret, G. Wörner, M. Fornari, Neogene and Quaternary ignimbrites in the area of Arequipa, Southern Peru: Stratigraphical and petrological correlations. *J. Volcanol. Geotherm. Res.* **154**, 251–275 (2006).
58. W. D. MacDonald, H. C. Palmer, A. L. Deino, P.-Y. Shen, Insights into deposition and deformation of intra-caldera ignimbrites, central Nevada. *J. Volcanol. Geotherm. Res.* **245–246**, 40–54 (2012).
59. E. McClelland, C. J. N. Wilson, L. Bardot, Palaeotemperature determinations for the 1.8-ka Taupo ignimbrite, New Zealand, and implications for the emplacement history of a high-velocity pyroclastic flow. *Bull. Volcanol.* **66**, 492–513 (2004).
60. T. Kidane, Y.-I. Otofuji, Y. Komatsu, H. Shibasaki, J. Rowland, Paleomagnetism of the Fentale-magmatic segment, main Ethiopian Rift: New evidence for counterclockwise block rotation linked to transtensional deformation. *Phys. Earth Planet. Inter.* **176**, 109–123 (2009).
61. E. Zanella, A. Cicchino, R. Lanza, Composite detrital and thermal remanent magnetization in tuffs from Aeolian Islands (southern Tyrrhenian Sea) revealed by magnetic anisotropy. *Int. J. Earth Sci.* **101**, 841–848 (2012).
62. D. Jeong, Y. Yu, S.-J. Doh, D. Suk, J. Kim, Paleomagnetism and U-Pb geochronology of the late Cretaceous Chisulryoung Volcanic Formation, Korea: Tectonic evolution of the Korean Peninsula. *Earth Planets Space* **67**, 66 (2015).
63. M. S. Petronis, A. R. Brister, V. Rapprich, B. van Wyk de Vries, J. Lindline, J. Mišurec, Emplacement history of the Trosky basanitic volcano (Czech Republic): Paleomagnetic, rock magnetic, petrologic, and anisotropy of magnetic susceptibility evidence for lingering growth of a monogenetic volcano. *Austrian J. Geosci.* **60**, 207–238 (2015).
64. M. S. Petronis, J. W. Geissman, W. C. McIntosh, Transitional field clusters from uppermost Oligocene volcanic rocks in the central Walker Lane, western Nevada. *Phys. Earth Planet. Inter.* **141**, 207–238 (2004).
65. E. McClelland, P. S. Erwin, Was a dacite dome implicated in the 9,500 b.p. collapse of Mt Ruapehu? A palaeomagnetic investigation. *Bull. Volcanol.* **65**, 294–305 (2003).
66. H. Tanaka, H. Hoshizumi, Y. Iwasaki, H. Shibuya, Applications of paleomagnetism in the volcanic field: A case study of the Unzen Volcano, Japan. *Earth Planets Space* **56**, 635–647 (2004).
67. A. Genevey, Y. Gallet, G. Boudon, Secular variation study from non-welded pyroclastic deposits from Montagne Pelée volcano, Martinique (West Indies). *Earth Planet. Sci. Lett.* **201**, 369–382 (2002).
68. N. M. King, J. W. Hillhouse, S. Gromme, B. P. Hausback, C. J. Pluhar, Stratigraphy, paleomagnetism, and anisotropy of magnetic susceptibility of the miocene stanislaus group, central sierra nevada and sweetwater mountains, California and Nevada. *Geosphere* **3**, 646–666 (2007).
69. G. M. Turner, B. V. Alloway, B. J. Dixon, C. B. Atkins, Thermal history of volcanic debris flow deposits on the eastern flanks of Mt. Taranaki, New Zealand: Implications for future hazards. *J. Volcanol. Geotherm. Res.* **353**, 55–67 (2018).
70. G. Fontana, C. Mac Niocaill, R. J. Brown, R. S. J. Sparks, M. Field, Emplacement temperatures of pyroclastic and volcaniclastic deposits in kimberlite pipes in southern Africa. *Bull. Volcanol.* **73**, 1063–1083 (2011).
71. K. Uno, K. Furukawa, H. Ando, T. Shinmura, M. Miyoshi, Instantaneous record of the geomagnetic field direction of various facies from pyroclastic flow deposits: Tests for consistency in paleomagnetic directions. *Phys. Earth Planet. Inter.* **235**, 96–106 (2014).
72. E. Zanella, G. De Astis, R. Lanza, Palaeomagnetism of welded, pyroclastic-fall scoriae at Vulcano, Aeolian Archipelago. *J. Volcanol. Geotherm. Res.* **107**, 71–86 (2001).
73. P. Roperch, A. Chauvin, J.-L. Le Pennec, L. E. Lara, Paleomagnetic study of juvenile basaltic–andesite clasts from Andean pyroclastic density current deposits. *Phys. Earth Planet. Inter.* **227**, 20–29 (2014).

Acknowledgments: We thank two anonymous reviewers for helpful suggestions. **Funding:** We acknowledge support from the Natural Sciences and Engineering Research Council of Canada and the Canadian Space Agency (A.M. and C.L.J.). B.L. was partly supported by CNES in the frame of the InSight mission and by the NEWTON project, funded by the European Union's Horizon 2020 research and innovation program under grant agreement 730041. C.L.J. also thanks the Green Foundation for Earth Sciences for support during a leave at the Institute of Geophysics and Planetary Physics, 2019–2020. **Author contributions:** A.M. led the synthesis of the magnetic field investigations reported here and wrote the main text. C.L.J. contributed to all aspects of the analysis and manuscript preparation. A.M. produced all the figures and tables with the exception of Fig. 4C (J.M.F.) and fig. S4 (B.L.). R.J.P. advised with the overall manuscript and helped with the geological analysis of the AP region. J.M.F. assisted in the mineralogical explanations related to excavation and magnetization of the pyroclastic flow. B.L. contributed to the discussion on magnetization and excavation due to impacting and published the model used in fig. S4. All authors revised the final manuscript. **Competing interests:** The authors declare that they have no competing interests. **Data and materials availability:** The MGS and MAVEN magnetic field data used in this study are archived in the Planetary Data System. All data needed to evaluate the conclusions in the paper are present in the paper and/or the Supplementary Materials. Additional data related to this paper may be requested from the authors.

Submitted 30 October 2019
Accepted 12 February 2020
Published 1 May 2020
10.1126/sciadv.aba0513

Citation: A. Mittelholz, C. L. Johnson, J. M. Feinberg, B. Langlais, R. J. Phillips, Timing of the martian dynamo: New constraints for a core field 4.5 and 3.7 Ga ago. *Sci. Adv.* **6**, eaba0513 (2020).

Science Advances

Timing of the martian dynamo: New constraints for a core field 4.5 and 3.7 Ga ago

A. Mittelholz, C. L. Johnson, J. M. Feinberg, B. Langlais and R. J. Phillips

Sci Adv **6** (18), eaba0513.
DOI: 10.1126/sciadv.aba0513